Title
Tunable Microporous Bimetallic Carboxylate-Pyrazolate Metal—Organic Frameworks for CO2 Capture

Journal
Journal of the American Chemical Society, 148(26)

ISSN
0002-7863

Authors
Yurdusen, Aysu
Malik, Pratibha
Mansouri, Asma
et al.

Publication Date
2026-06-24

DOI
10.1021/jacs.6c07605

Peer reviewed

JACS
JOURNAL OF THE AMERICAN CHEMICAL SOCIETY
pubs.acs.org/JACS
Article

Tunable Microporous Bimetallic Carboxylate-Pyrazolate Metal–Organic Frameworks for CO_2 Capture

Aysu Yurdusen,[†] Pratibha Malik,[†] Asma Mansouri, Iurii Dovgaliuk, Matthew Garvin, Ah-Young Song, Alireza Pourghaderi, Xin Jin, Luke Stuart, Debanjan Chakraborty, Shyamapada Nandi, Lokuge Aravindani Fernando, Anthony Beauvois, Valérie Briois, Jeffrey A. Reimer, Susana Garcia, Berend Smit, Georges Mouchaham,* and Christian Serre*

Cite This: https://doi.org/10.1021/jacs.6c07605

ABSTRACT: Herein, we report two heterometallic ultramicroporous metal–organic frameworks, MIP-212(Al/Cu) and MIP-212(Al/Zn) (MIP stands for Materials from Institute of Porous Materials of Paris), synthesized via a hard–soft acid–base design strategy. In these robust pyrazolate–carboxylate architectures, pyrazolates selectively coordinate Cu^{2+} or Zn^{2+}, while carboxylates bind Al^{3+}, generating chain-based inorganic building units built up from connected M^{2+}-pyrazolate polyhedra and μ_2–OH-corner-shared AlO_6 octahedra, respectively. The resulting structures feature dual ultranarrow tunnel-like pores, one decorated with μ_2–OH groups. MIP-212(Al/Cu) combines pore confinement with Cu^{2+} open metal sites (OMS) to deliver benchmark-level CO_2 uptake at low pressure (2.30 mmol g^{-1} at 0.15 bar, 298 K) and a CO_2/N_2 Ideal Adsorbed Solution Theory (IAST) selectivity of ∼30. However, the OMS also imparts marked hydrophilicity, diminishing CO_2 uptake under humid conditions. Markedly, replacing octahedral Cu^{2+} with tetrahedral Zn^{2+} centers in MIP-212(Al/Zn) suppresses OMS while preserving framework topology, resulting in significantly lower water affinity (up to ca. 4-fold reduction at 0.2 bar of H_2O) and superior CO_2 breakthrough performance at 50% RH. These findings demonstrate that metal coordination geometry is a powerful lever to modulate hydrophilicity and sorption behavior in MOFs, enabling the rational design of sorbents for efficient CO_2 capture under realistic, moisture-rich environments.

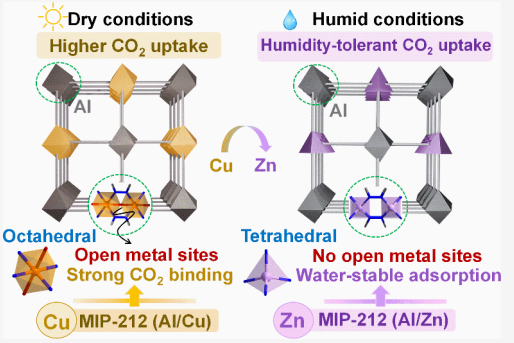

1. INTRODUCTION

Carbon capture technologies are essential for reducing anthropogenic CO_2 emissions.[1] Although more than 50 Mt of CO_2 are currently captured each year, this figure is projected to reach approximately 435 Mt by 2030.[2] Industrial systems rely on amine-based absorbents, but their high regeneration energy and poor stability limit large-scale deployment. These drawbacks drive the development of robust solid sorbents with high CO_2 capacity, selectivity, and fast cycling kinetics to enable low-carbon energy technologies.[3] In this respect, metal–organic frameworks (MOFs), a class of micro- or mesoporous hybrid solids, have emerged, among others.[4] Their unprecedented versatile character endows some of them with high CO_2 uptake capacities as well as the possibility to tune their selectivity in the presence of impurities (including moisture) and to enhance their thermal/chemical stability. Recently, they have indeed shown significant progress in this regard.[5−8]

Among them, the ultramicroporous Zn-oxalate-triazolate CALF-20 (CALF: Calgary Frameworks) stands out as a 'game changer' benchmark sorbent due to its high CO_2 working capacity in postcombustion conditions, long-term stability, easy thermal regeneration, and scalability at the multiton production.[7,9] Notably, it maintains its CO_2 capture performance up to ∼30% RH before exhibiting a gradual decrease at higher humidity levels. In addition, cost-effective Al-based MOFs such as Al-formate (AlF),[10] MIL-120(Al)[8] (MIL: Materials of Institute Lavoisier), MIL-160(Al)[11,12] and MIL-53(Al)-NH_2[13] have demonstrated strong performance for postcombustion CO_2 separation. However, designing new MOF families that combine benchmark-level CO_2 uptake with retained performance under realistic humid conditions through rational and transferable structural design principles remains an open challenge.

Carboxylate-based MOFs are among the most common structures owing to their predictable design, tunable top-

Received: April 13, 2026
Revised: June 12, 2026
Accepted: June 16, 2026

ologies, and ease of functionalization. MOFs constructed from 'hard' carboxylate-based linkers and "hard" high valence metal cations (Al^{3+}, Fe^{3+}, Zr^{4+}, Ti^{4+}···) show good hydrothermal stability under neutral or acidic conditions, although they show limited durability in basic environments.[5,14−18] Among them, Al-based MOFs attract much attention because of the relatively low cost and abundance of this metal. Of the different possible inorganic building units (IBUs) (i.e., Al-oxo-trimer form),[19,20] Al^{3+}, once combined with carboxylates, usually form Al-hydroxy-chains, the most thermodynamically stable configuration,[14] leading to 1D channels, as seen in MIL-53(Al)-s[19,21−24] or CAU-10(Al)/MIL-160(Al)[12,25] (CAU: Christian-Albrechts-University), which have been extensively studied for adsorption-related applications.[23,25] Experimental and computational studies revealed that CO_2 adsorption in such structures is primarily driven by interactions between CO_2 and the μ_2-hydroxyl groups of Al chains.[24] Azolates are another common class of ligands used in MOF construction, although they are more expensive and, in most cases, less scalable than carboxylates, when combined with low valence metal ions (Zn^{2+}, Ni^{2+}···). Due to their high basicity, nitrogen atoms on the heterocycle bind strongly to (soft) transition metal ions, enhancing the framework's stability, particularly under basic conditions with divalent metal ions[18,26]

Combining these two functionalities within a single bifunctional pyrazolate-carboxylate (PyC) linker, where the pyrazolate selectively coordinates M^{2+} and the carboxylate binds Al^{3+} according to the hard−soft acid−base (HSAB) principle, is an effective strategy for designing a ligand that can selectively bind to both metal ions. The acid−base (HSAB) principle enables the construction of stable bimetallic MOFs featuring two chemically distinct IBUs within a single topology, providing promising candidates for CO_2 uptake applications.[15,27,28] However, existing bimetallic PyC MOFs are predominantly assembled from discrete cluster-based IBUs.[29] Furthermore, the ability to generate extended chain-based structures where M^{2+} coordination geometry can be systematically varied to tune open metal site formation, CO_2 affinity, and moisture tolerance within an isoreticular series has not yet been demonstrated.

Here, we report a novel bimetallic heterofunctional MOF, MIP-212(Al/Cu) (MIP stands for Materials from Institute of Porous Materials of Paris), formulated as $[AlCu(\mu_2{-}OH)(PyC)_2]$·solvent, constructed from both $Al(OH)_2O_4$ and CuN_4O_2 chains bridged by H_2PyC, a structural motif distinct from the discrete cluster-based IBUs of prior PyC frameworks, bearing, respectively, polar μ_2−OH groups and potentially accessible Cu(II) sites upon activation (removal of coordinated solvent molecules), both known to present high affinity toward CO_2 molecules.[30] The combination of pore confinement and accessible OMS enables MIP-212(Al/Cu) to show a high CO_2 uptake at ambient temperature and low pressure (ca. 2.30 mmol/g at 0.15 bar), approaching the performance of benchmark MOF sorbents, such as CALF-20 and MIL-120(Al)[7,8] with a good CO_2/N_2 IAST estimated selectivity of ca. 30 at 1 bar. Dynamic breakthrough experiments further confirm its strong performance, with a CO_2 sorption capacity of 1.59 mmol/g at 0.15 bar and 303 K in dry conditions. These results are consistent with the "Process-Informed design of tailor-made sorbent materials (PrISMa)" platform prediction identifying MIP-212(Al/Cu) as a top performer in temperature and temperature-vacuum swing adsorption (TSA and TVSA, respectively)-based carbon capture processes.[31] Despite these advantages, the presence of OMS in MIP-212(Al/Cu) imparts a pronounced hydrophilicity, resulting in decreased CO_2 uptake under wet conditions. As recent studies have shown the impact of the nature of the divalent metal ion on the water sorption properties of the MOF,[32] and given that Zn^{2+} ions preferentially adopt tetrahedral coordination environments when coordinated by PyC^{2-},[33] Cu^{2+} was substituted with Zn^{2+} to suppress the OMS formation. The resulting MIP-212(Al/Zn) retains the beneficial confinement and μ_2−OH functionality without the penalty in CO_2 performance observed in humid conditions for MIP-212(Al/Cu). Although single-component isotherms show modestly lower CO_2 uptakes (ca. 1.40 mmol/g at 0.15 bar and 3.45 mmol/g at 1 bar), dynamic breakthrough experiments under relevant capture conditions (15% CO_2, 83% N_2, 50% RH, 30 °C) reveal that MIP-212(Al/Zn) outperforms MIP-212(Al/Cu) (0.84 vs 0.76 mmol g^{-1}, respectively) demonstrating that the dry-performance/moisture-tolerance trade-off can be rationally navigated through deliberate control of M^{2+} coordination geometry. Collectively, these results establish M^{2+} coordination geometry as a powerful and transferable design principle for both CO_2 adsorption and water tolerance, establishing a clear design strategy for next-generation moisture-tolerant MOF-based sorbents.

2. RESULTS AND DISCUSSION

Synthesis, Structural Analysis, and CO_2 Sorption Performance

MIP-212(Al/Cu) was synthesized via a solvothermal route, reacting 0.3 mmol $Al(NO_3)_3{\cdot}9H_2O$, 0.6 mmol $Cu(NO_3)_2{\cdot}2.5H_2O$, and 0.31 mmol H_2PyC in a *N,N*-dimethylformamide (DMF)−water−ethanol mixture (1:1:2 (v/v) %) in the presence of acetic acid in sealed Pyrex tubes at 75 °C for 2 days. The collected purple solid was then thoroughly washed with DMF and ethanol and later dried under vacuum (<30% yield, based on H_2PyC). Details are provided in the Supporting Information (Section S2). Additionally, the repeatability of the synthesis protocol was evaluated by using CO_2 sorption measurements from eight independently synthesized batches. Details of these can be found in the Supporting Information (Section S15).

The washed and activated MIP-212(Al/Cu) samples were analyzed by means of a wide set of characterization techniques, including high-resolution laboratory powder X-ray diffraction (HR-PXRD), variable-temperature powder X-ray diffraction (VT-PXRD), Fourier transform infrared (FTIR), solid-state NMR (ssNMR), thermal gravimetric analysis (TGA), N_2, CO_2, water sorption analysis, and breakthrough measurements.

HR-PXRD (Cu $K\alpha_1$ = 1.5406 Å) data were collected to assess the structural features of MIP-212(Al/Cu). As reported in literature, reacting Cu^{2+} with H_2PyC may result in one of the several possible configurations such as Cu_3-oxo-cluster ($[Cu_3(\mu_3{-}O/OH)(PyC)_3]^{n-}$),[17,28,34] a 12-membered ring cluster ($[Cu_{12}(\mu_2{-}OH)_{12}(PyC)_{12}]$),[18] a 4-membered cluster with the pyrazole rings forming a tetrahedron ($[Cu_4(PyC)_4]$),[35] or copper chains ($[Cu(PyC)_2{\cdot}H_2O]$).[36] Furthermore, reacting with both Al^{3+} and Cu^{2+} ions with H_2PyC, one could expect to obtain the mesoporous MOF-919 built of $[Cu_3O(OH)_3(PyC)_3(H_2O)_6]$ metalloligand and $[Al_3O(OH)]^{6+}$ oxoclusters delimiting mesoporous cages of different topologies.[37] Contrary to these expectations, HR-PXRD analysis demonstrated that MIP-212(Al/Cu) crystallizes in a distinct

https://doi.org/10.1021/jacs.6c07605
J. Am. Chem. Soc. XXXX, XXX, XXX−XXX

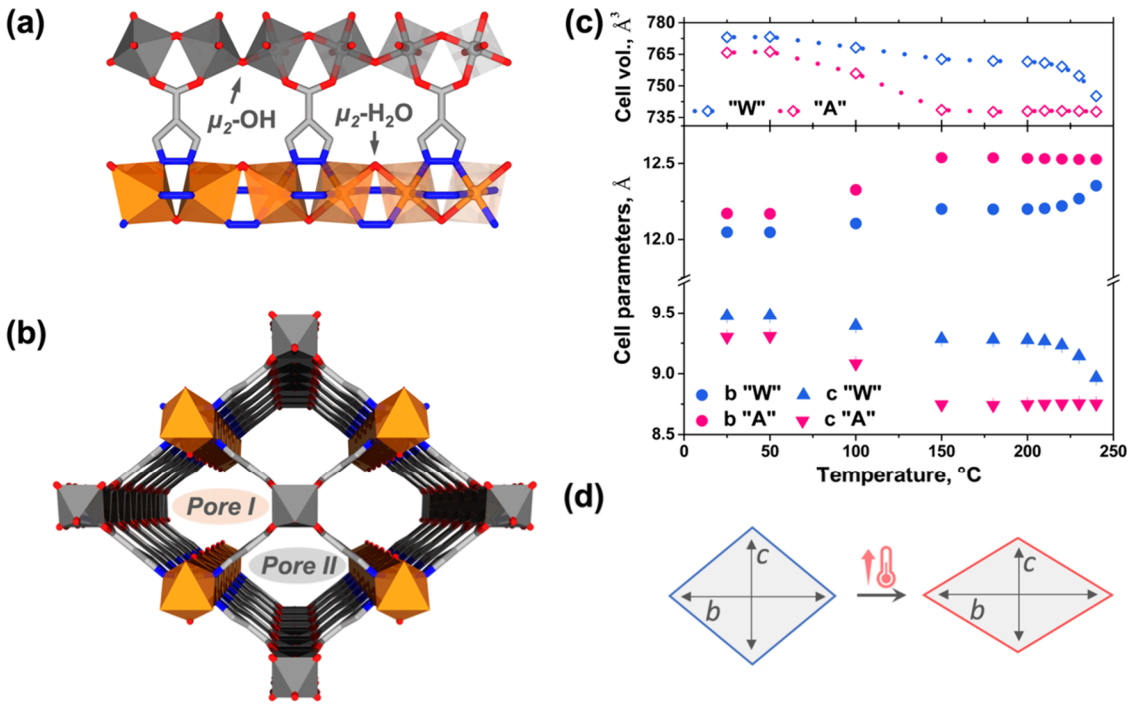

Figure 1. Representation of MIP-212(Al/Cu) crystal structure: (a) $AlO_4(OH)_2$ and $CuN_4(H_2O)_2$ chains linked by PyC ligand; and (b) projection of the MIP-212(Al/Cu) crystal structure along [100]: AlO_6 − gray polyhedron; $CuN_4(O)_2$ − orange polyhedron; N − blue; O − red; hydrogen atoms and guest molecules are not shown. (c) Temperature dependence of the unit cell parameters and volumes of only washed ("W") and thermally activated ("A") MIP-212(Al/Cu) samples prior to analyses. (d) Schematic representation of the channel opening before and after thermal activation.

chain-based structural framework. The HR-PXRD analysis revealed that MIP-212(Al/Cu) or $[AlCu^{II}(\mu_2{-}OH)(PyC)_2]\cdot xH_2O$ crystallizes in the orthorhombic *Pmma* space group (n°51) with a = 6.7709 (4) Å, b = 12.0482 (7) Å, c = 9.4765 (6) Å, and V = 773.1 Å^3 for MIP-212(Al/Cu) washed but not thermally activated. The structure consists of two types of one-dimensional chains built from $AlO_4(OH)_2$ and $CuN_4(H_2O)_2$ octahedra, which are aligned along the [100] crystallographic direction (Figure 1a). These chains are linked by PyC^{2-} linkers, where the pyrazole N atoms coordinate to Cu^{2+} centers and the carboxylate O atoms to Al^{3+} ions. Such connectivity of the chains resembles the structure of MIL-53.[21,38] However, in the case of heterometallic MIP-212(Al/Cu), it leads to the formation of two distinct one-dimensional pores (**I** and **II**) with different chemical environments (Figure 1b). The ultramicroporous, lozenge-shaped channels of pore **I** are formed by copper chains, which are at their closest position along the c axis coordinated with water/solvent molecules, while pore **II** is formed of aluminum chains coordinating with μ_2−OH. Moreover, to evaluate the structural changes in MIP-212(Al/Cu) upon thermal activation, VT-PXRD patterns were collected. The results from the VT-PXRD analysis reveal that the activated MIP-212(Al/Cu) maintains the same structure with slight variations of the unit cell parameters, and the cell volume (V = 773.1 Å^3 for MIP-212(Al/Cu) washed and measured at 25 °C vs V = 737.7 Å^3 for MIP-212(Al/Cu) activated at 240 °C) (Figure 1c,d). However, the removal of the free linker and the coordinated water from the washed sample upon heating demonstrates that the unit cell parameters b and c, and the cell volume after 200 °C, start to approach a plateau at around 240 °C. For morphological and elemental composition analysis (Al and Cu), SEM imaging and EDX analysis were recorded (Supporting Information, Section S5, Figure S14). Remarkably, the thermally preactivated MIP-212(Al/Cu) reached these values at a much lower temperature, 150 °C, suggesting that the removal of the free linker as well as some fraction of water (solvent) molecules induces these changes (Supporting Information, Section S10). Furthermore, to gain more insights into the "activated" framework, we determined the crystal structure of an *ex situ*-activated sample based on HR-PXRD data (Supporting Information, Section S3, Figures S1 and S2). These results indicate that, despite all our attempts, the maximum attainable fraction of Cu-OMS (and a lower fraction of coordinated water) is approximately 60%, which was also confirmed by Rietveld refinement (Supporting Information, Section S4, Figures S5 and S6), where the experimental activation process was mimicked. All our attempts to reach a higher degree of dehydration led to a collapse of the structure due to a lack of compatibility in the environment of the fully dehydrated copper ions, since it is inherently challenging for copper ions to form a tetrahedral coordination environment, given the likelihood of Cu(II) to be reduced to Cu(I). Additionally, ssNMR (Supporting Information, Section S19, Figure S63) further verifies reversible removal and recoordination of water upon activation and rehydration, consistent with previous reports showing 50−70% water loss.[31] Finally, the refinement of the crystal structure after activation was successfully performed (Supporting Information, Section S4). It is revealed that depending on the fraction of coordinated water molecules, the diameter of channel **I** varies between ∼6 × 3.5 Å and ∼6 × 5 Å, while the diameter of channel **II**, where aluminum chains are linked along the c-axis coordinating with μ_2−OH facing the center of the channel, is ∼6 Å × 5 Å (values are estimated from the structure solved before activation (Supporting Information, Section S4, Figure S7)). This behavior demonstrates the

https://doi.org/10.1021/jacs.6c07605
J. Am. Chem. Soc. XXXX, XXX, XXX−XXX

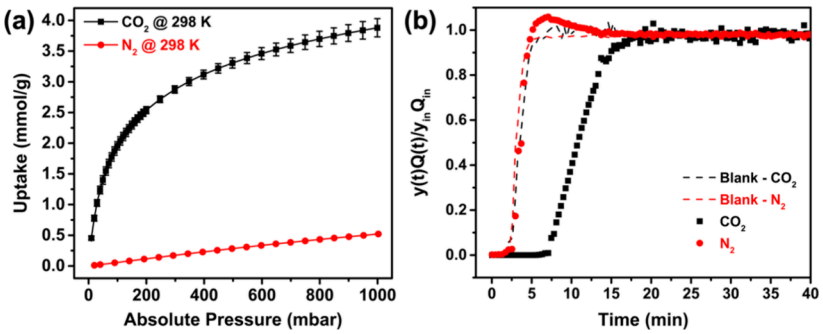

Figure 2. (a) CO_2 and adsorption isotherm (averaged on 8 measurements) and N_2 adsorption isotherm measured at 298 K and 1 bar and (b) breakthrough curves for 15% CO_2, 85% N_2 dry gas mixture measured at 303 K (gas feed at 10 mL/min).

breathing effect of the MIP-212(Al/Cu) and its dependence on the pore content/loading. Interestingly, the thermally activated MIP-212(Al/Cu) recovers its initial structure (but without any free linker) after soaking in water, as confirmed by HR-PXRD analysis of a water-soaked capillary (Supporting Information, Section S3, Figure S2).

Prior to gas sorption studies, FTIR spectra of washed-MIP-212(Al/Cu) were recorded (Supporting Information, Section S7, Figure S18). It was observed that repeated washing with polar solvents such as DMF or ethanol was not sufficient to completely remove the unreacted linker from the pores, therefore making thermal activation necessary (240 °C for 7 h). PXRD analysis further confirmed that the material remains crystalline after treatment at 240 °C for 7 h, identifying this temperature as optimal for activation. Details of the optimization of the activation process are provided in the Supporting Information, Section S7 (the obtained solid is labeled as the "activated" form). Furthermore, MIP-212(Al/Cu) was washed with dimethyl sulfoxide (DMSO) to identify a greener alternative for the washing and the activation process of MIP-212(Al/Cu). DMSO-washed samples achieved full pore accessibility upon activation at 150 °C, 90 °C lower than the 240 °C required for DMF/ethanol-washed samples, representing a significant reduction in energy input. The CO_2 uptake of the DMSO-washed sample activated at 150 °C (2.11 mmol/g at 0.15 bar) is within experimental error of the standard DMF/ethanol-washed sample activated at 240 °C (2.30 mmol/g), confirming that comparable activation is achieved at substantially milder conditions. These results establish DMSO washing as a viable and more energy-efficient alternative for the activation of MIP-212(Al/Cu).[13] In continuation of this approach, we also explored tentatively a greener synthesis route for MIP-212(Al/Cu) by replacing DMF with a dynamic solvent system (DSS) of acetic acid and 1-butanol, known as a dynamic solvent (Supporting Information, Section S8). Although this modification led to a slightly lower yield, the MOF was still successfully synthesized, and its CO_2 adsorption performance remained comparable to that obtained from the conventional DMF-based synthesis. Importantly, this greener synthetic strategy could also be applied to MIP-212(Al/Zn), highlighting its broader applicability.

N_2 sorption analysis performed at 77 K illustrates that MIP-212(Al/Cu) is formed of micropores following the typical features of IUPAC type I isotherm (Supporting Information, Section S7, Figure S20), with a calculated BET surface area of 618 ± 40 m^2/g. TGA of both washed and activated MIP-212(Al/Cu) under O_2 environment up to a temperature of 600 °C (Supporting Information, Section S6, Figure S16) shows two weight losses: 17.4% below ∼100 °C due to solvent and water removal, and ∼48.7% at ∼315 °C corresponding to linker decomposition and initiation of the framework degradation to metal oxides. Furthermore, the VT-PXRD analysis conducted under air shows that MIP-212(Al/Cu) retains its crystallinity up to 280 °C but starts to decompose upon prolonged exposure (Supporting Information, Section S10, Figures S37−S39). In addition, the hydrolytic stability of MIP-212(Al/Cu) was confirmed by stirring MIP-212(Al/Cu) in deionized water at room temperature (1.1 mg/mL) for several days. No crystallinity loss or decrease in adsorption capacity was observed (Supporting Information, Section S9, Figure S35).

The unique combination of short carboxylate−pyrazolate linkers and the bimodal pores with two distinct chemical environments (μ_2−hydroxyl groups coordinating to Al chains and Cu open metal sites) encouraged the investigation of the CO_2 sorption behavior of MIP-212(Al/Cu). Single-component N_2 and CO_2 sorption measurements reveal that MIP-212(Al/Cu) demonstrates a comparably higher CO_2 uptake than N_2 at 298 K. Indeed, the CO_2 sorption isotherms (averaged on 8 measurements) showed uptakes of ≈2.30 ± 0.07 mmol/g at 0.15 bar and ≈3.88 ± 0.15 mmol/g at 1 bar (Figure 2a and Figure S48), remarkably, comparable to the benchmark sorbent, CALF-20 (Figure S45).[7] Compared to other poly-(pyrazolate)-based MOFs under equivalent experimental conditions, these results show that MIP-212(Al/Cu) is one of the best performers.[5,15,16,18,39] Also, it is observed that MIP-212(Al/Cu) shows a better CO_2 uptake capacity at 1 bar when compared to MIL-53(Al) and its isoreticular analogues (i.e., MIL-53(Al)-X, X = $-NH_2$, $-NO_2$, −Cl, −Br, $-CH_3$), even outperforming MIL-53(Al)-NH_2 at 0.15 bar.[40]

These results demonstrate that integrating two distinct chemical environments within a single framework enhances the CO_2 uptake capacity of a MOF. Utilizing the Clausius−Clapeyron equation on the single-component CO_2 adsorption isotherms performed at 300, 310, and 320 K, the zero-coverage heat of adsorption was estimated as −36.8 kJ mol^{-1} (Supporting Information, Section S11, Figure S41), revealing the relatively low-energy demand for the regeneration process of MIP-212(Al/Cu). Using the IAST model, the CO_2:N_2 selectivity of MIP-212(Al/Cu) was estimated as ca. 30 for 15CO_2:85N_2 at 298 K and 1 bar (Supporting Information, Section S12, Figure S43). A comparison with the benchmark sorbents such as CALF-20, AlF, and MIL-120(Al) underscores the competitive performance of MIP-212(Al/Cu) for post-combustion CO_2 capture (Supporting Information, Section

https://doi.org/10.1021/jacs.6c07605
J. Am. Chem. Soc. XXXX, XXX, XXX−XXX

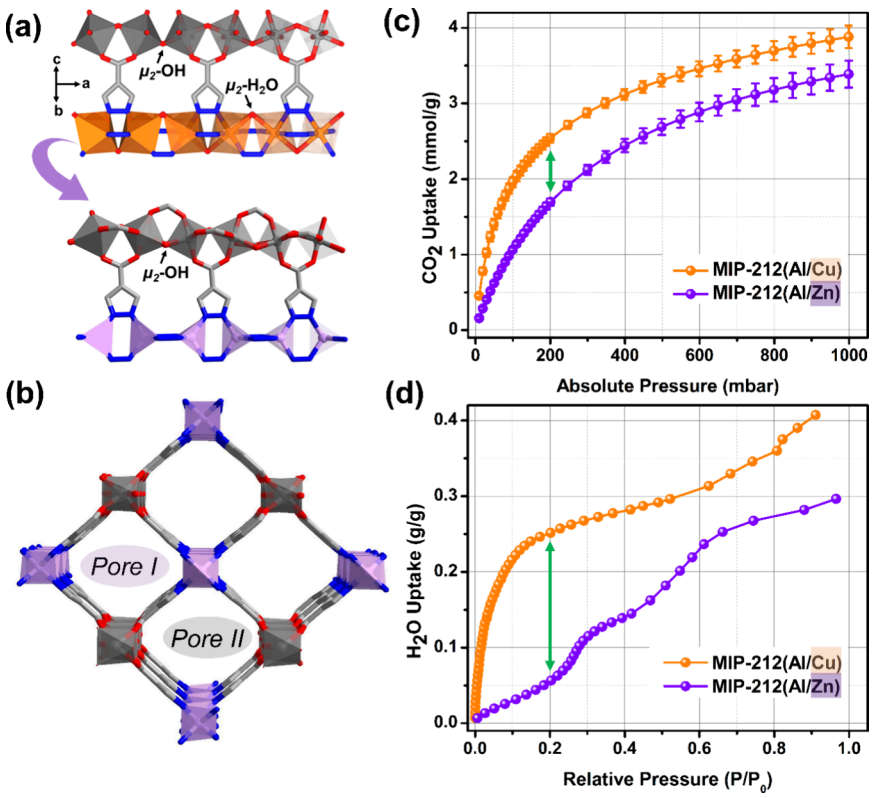

Figure 3. (a) Structural representation illustrating the substitution of Cu chains by Zn chains in the MIP-212 framework. (b) Crystal structure of MIP-212(Al/Zn) displaying two distinct pore domains with AlO_6 – gray polyhedron; ZnN_4 – purple polyhedron; N – blue; O – red (c) CO_2 adsorption isotherms of MIP-212(Al/Cu) and MIP-212(Al/Zn) at 298 K. (d) H_2O adsorption isotherms of MIP-212(Al/Cu) and MIP-212(Al/Zn) at 298 K.

S13, Figure S45).[7,8,10] Water sorption analysis performed at 298 K reveals that MIP-212(Al/Cu) possesses a moderate hydrophilic behavior at low relative pressures ($P/P_0 < 0.2$) that arises very likely from the presence of OMS and the μ_2−OH groups (Figure S46 and Figure 3d). Furthermore, to assess the CO_2/N_2 separation performance of MIP-212(Al/Cu) under realistic conditions, dynamic breakthrough experiments were carried out using CO_2:N_2 (15:85) and CO_2:N_2:H_2O mixtures (Supporting Information, Section S18). The dry breakthrough experiments (Figure 2b) confirm the selectivity shown by the single-component isotherms (Figure 2a). The CO_2 breakthrough occurs after ∼7 min and is characterized by a less steep adsorption front than that of the N_2. The latter breakthrough of CO_2 and the roll-up observed in N_2 confirms that CO_2 is the strongest adsorbed component in the binary mixture. Repeated runs showcased the reproducibility of the breakthrough curves (Supporting Information, Section S18), with only a little variation observed. Under dry conditions, MIP-212(Al/Cu) has an average capacity of 1.59 mmol/g, which is lower than that observed in the CO_2 isotherm (2.30 mmol/g at 0.15 bar, Figure 2a). The lower CO_2 uptake measured in the breakthrough experiments relative to the equilibrium adsorption isotherms may be attributed to a combination of factors. In particular, the activation procedure used prior to the breakthrough tests (without vacuum) differed slightly from that employed for the isotherm measurements (under vacuum) and may have resulted in a lower degree of sample activation. Furthermore, kinetic and mass-transfer effects may also contribute to the reduced apparent adsorption capacity (details of the activation conditions can be found in Supporting Information, Section S7). Additionally, heat effects due to the exothermic nature of the adsorption step might negatively impact uptake. This study, combined with the predictions from the PrISMa platform, is an illustration that one can benefit from the relatively high CO_2 sorption capacity of MIP-212(Al/Cu) when operated under TSA regeneration conditions.[31]

To further understand the adsorption behavior and the interaction mechanisms within MIP-212(Al/Cu), density functional theory (DFT) calculations were performed. The DFT binding energy results in Table S11 (Supporting Information, Section S16) demonstrate that, for the MIP-212(Al/Cu)-activated structure, CO_2 molecules energetically favor adsorption in Pore **I**. In contrast, H_2O exhibits strong adsorption sites in both pores **I** and **II**: in pore **I** at the Cu open metal sites, and in pore **II** at the μ_2−OH groups pointing toward the pore channel, as shown in Supporting Information, Section S16, Figure S50. This leads to a competitive adsorption between CO_2 and H_2O in pore **I**. Although previous studies have reported that coordinated water at open metal sites may still serve as favorable adsorption sites for CO_2,[41] the occupation of pore space by H_2O still reduces the overall CO_2 adsorption capacity. Complementary grand-canonical Monte Carlo (GCMC) simulations using the universal force field (UFF) were conducted to compare with the experimental adsorption isotherms (Supporting Information, Section S17, Figure S52). At low pressure, CO_2 preferentially adsorbs on the Cu rods, which are reasonably well described within the UFF framework, resulting in good agreement between the simulated and experimental isotherms.

https://doi.org/10.1021/jacs.6c07605
J. Am. Chem. Soc. XXXX, XXX, XXX−XXX

It is to be noted that in GCMC, gas uptake overestimation at low pressure can arise from the strong polarizing nature of Al centers.[42] The remaining deviation at higher pressures can be attributed to the use of a rigid-framework approximation in the GCMC simulations, which does not fully capture the structural flexibility of MIP-212(Al/Cu) under such conditions.

It is important to note that our investigations indicate that Cu centers are predominantly present in the cupric oxidation state. However, *in situ* preliminary X-ray absorption spectroscopy (XAS) reveals that upon heating, around 9% of the Cu^{2+} undergoes partial reduction to Cu^{+} (Supporting Information, Section S20, Figure S70) prior to framework degradation (at T > 240 °C) (for more details, Supporting Information, Section S20) and eventual formation of Cu°.

Although MIP-212(Al/Cu) exhibits excellent CO_2 uptake and selectivity under dry conditions (15% CO_2, 85% N_2), its moderate water uptake capacity at low relative pressures arising from the presence of Cu open metal sites limits its performance under humid conditions. To overcome this limitation, while preserving the favorable confinement and μ_2−OH−CO_2 interactions,[24] we designed a derivative framework, MIP-212(Al/Zn) (Figure 3a,b). In this material, Zn^{2+} replaces Cu^{2+}, adopting a tetrahedral coordination with the PyC^{2-} linker that prevents the formation of open metal sites. This subtle yet effective modification reduces hydrophilicity while maintaining the framework stability and CO_2 affinity.

MIP-212(Al/Zn) was synthesized via the same solvothermal method as MIP-212(Al/Cu), using $Al(NO_3)_3{\cdot}9H_2O$ and $Zn(NO_3)_2{\cdot}6H_2O$ as metal precursors. The obtained solid product was activated and dried under vacuum overnight (<45% yield, based on H_2PyC (Supporting Information Section S2)). The repeatability of the Zn analogue synthesis was evaluated using CO_2 sorption measurements from eight independently prepared batches, with full details provided in (Supporting Information, Section S15).

MIP-212(Al/Zn) was characterized using the same methods as MIP-212(Al/Cu). FTIR indicated that multiple washes with polar solvents were insufficient to remove residual linker, requiring thermal activation at 240 °C for complete activation following the same procedure as employed for MIP-212(Al/Cu) (Supporting Information, Section S7, Figure S19). N_2 sorption at 77 K revealed the microporous nature of MIP-212(Al/Zn), showing the characteristic features of a Type I isotherm and a BET surface area of 585 ± 52 m^2/g (Supporting Information, Section S7, Figure S21). SEM imaging and EDX analysis were also performed to examine the morphology and confirm the elemental composition (Al and Zn) (Supporting Information, Section S5, Figure S15). TGA performed under an O_2 environment up to 600 °C showed thermal stability up to 400 °C, with ∼14% weight loss from solvent removal and ∼45.7% from linker decomposition (Supporting Information, Section S6, Figure S17). Hydrolytic stability tests in deionized water at room temperature confirmed no loss of crystallinity after several days (Supporting Information, Section S9, Figure S36). The main difference between MIP-212(Al/Zn) and MIP-212(Al/Cu) lies in their framework structure, as revealed by XRD analysis. HR-PXRD analysis suggests that washed MIP-212(Al/Zn) adopts the *Ibam* space group (n°72) (the Le-Bail plot, Supporting Information, Section S4, Figures S8−S12). After activation at 240 °C under dynamic vacuum, significant changes in the PXRD pattern were observed, indicating a structural transformation. *In situ* synchrotron powder X-ray diffraction (SRPXRD) study revealed a high-temperature single phase in the *Ibam* space group, with a reversible transition upon cooling to a distorted low-symmetry form. Due to the complexity of the room-temperature structure, only lattice parameters were extracted, while full refinement was achieved for the high-temperature phase only; further details are discussed in the Supporting Information, Section S4. Tetrahedral coordination of Zn^{2+} with PyC^{2-} has been previously reported in several frameworks. For example, in NUS-5, each Zn^{2+} center binds two nitrogen atoms from adjacent ligands and two oxygen atoms, one from a coordinated water molecule and one from a neighboring ligand, yielding a 2D layered framework.[33] Additionally, tetrahedral zinc coordination was observed in two distinct IBUs, $[Zn_4(\mu_4{-}O)(CO_2)_6]$ and $[Zn_4(\mu_4{-}O)(N_2)_6]$, reported in a related study.[43] Consistently, in MIP-212(Al/Zn), Zn^{2+} adopts a tetrahedral coordination environment in the presence of PyC^{2-}, preventing OMS formation upon activation.

MIP-212(Al/Zn)-HT resembles the formation of two types of lozenge-like 1D openings (pores **I** and **II**) as in MIP-212(Al/Cu). The pore apertures in MIP-212(Al/Zn) measure 5.8 × 4.9 Å (pore **I**) and 6.1 × 5.1 Å (pore **II**) and do not form the Zn-OMS upon heating (Figures 1b and 3b and Figure S13).

The single-component CO_2 sorption isotherms (averaged on eight measurements) showed uptakes of ≈1.41 ± 0.03 mmol/g at 0.15 bar and ≈3.4 ± 0.174 mmol/g at 1 bar (Figure 3c and Supporting Information, Section S15, Figure S49). By using the Clausius−Clapeyron equation on the single-component CO_2 adsorption isotherms performed at 300, 310, and 320 K, the zero-coverage heat of adsorption was estimated as −30.5 kJ mol^{-1} (Supporting Information, Section S11, Figure S42) for MIP-212(Al/Zn). Using the IAST model, the CO_2:N_2 selectivity of MIP-212(Al/Zn) was estimated to be ca. 32 for $15CO_2$:$85N_2$ at 298 K and 1 bar (Supporting Information, Section S12, Figure S44).

The water sorption isotherm of MIP-212(Al/Zn) follows a two-step pore-filling mechanism (Figure 3d). This behavior is supported by the crystal structure refinement and DFT calculations. It revealed that MIP-212(Al/Zn) consists of two pores with dimensions of 5.8 Å × 4.9 Å (pore **I**) and 6.1 Å × 5.1 Å (pore **II**). DFT calculations further support this interpretation by identifying two distinct H_2O adsorption environments in MIP-212(Al/Zn), with binding energies of −35.82 and −46.77 kJ mol^{-1} for pores **I** and **II**, respectively, as shown in Tables S11 and S12 (Supporting Information, Section S16). The difference in binding energies between these adsorption sites is consistent with the experimentally observed two-step adsorption isotherm.

Moreover, the second step and the associated hysteresis (Supporting Information, Section S14, Figure S47) together with the slightly incomplete closure of adsorption and desorption branches are likely attributed to the slight flexibility of MIP-212(Al/Zn), evidenced by variable-temperature *in situ* SRPXRD measurements (Supporting Information Section S4.3), rather than to capillary condensation, as both pore diameters are smaller than the critical pore diameter required for capillary condensation, thereby excluding the capillary condensation mechanism ($D_{critical}$ = 2 nm at 298 K).[44] While MIP-212(Al/Cu) shows a comparatively high uptake at low relative pressures, MIP-212(Al/Zn) adsorbs almost one-quarter of the water MIP-212(Al/Cu) adsorbs at 0.2 bar. Further understanding of this difference will require dedicated

https://doi.org/10.1021/jacs.6c07605
J. Am. Chem. Soc. XXXX, XXX, XXX−XXX

structural studies with humidity control, which is beyond the scope of this work.

The breakthrough results demonstrated that despite MIP-212(Al/Cu)'s high CO_2 performance under dry conditions, it exhibits a drastic loss (i.e., 53%) in its CO_2 sorption capacity at 50% RH. In sharp contrast, MIP-212(Al/Zn) shows only a moderate decrease (i.e., 28%) under the same conditions (Figure 4 and Supporting Information, Section S18, Figures S59–S61). To understand the enhanced CO_2 adsorption of MIP-212(Al/Zn), particularly under humid conditions, we investigated the interaction of CO_2 with the framework using solid-state ^{13}C NMR and DFT calculations. NMR spectra of the material dosed with 15% ^{13}C-enriched CO_2 revealed a single resonance at 123 ppm, consistent with physisorbed CO_2 within the pore channels. The corresponding ^{13}C CPMAS spectrum with a short 500 μs contact time showed the same CO_2 resonance alongside unchanged linker carbons, indicating no carbonate or bicarbonate formation (Supporting Information, Section S19, Figures S64 and S65). Moreover, DFT calculations further suggest that tetrahedrally coordinated Zn^{II} centers lack OMS, weakening H_2O adsorption in pore **I**. Water molecules preferentially occupy pore **II**, while CO_2 binds similarly in both pores (Supporting Information, Section S16, Table S12), explaining why competitive adsorption of CO_2 in pore **I** enhances the overall CO_2 uptake of MIP-212(Al/Zn) compared to MIP-212(Al/Cu) under humid conditions.[45] In contrast to MIP-212(Al/Cu), where Cu sites are well described, UFF-based GCMC simulations for MIP-212(Al/Zn) overestimate low-pressure CO_2 uptake because at low pressure, CO_2 molecules mainly adsorb on the Al rods in pore **II**, which are poorly represented by the force field, leading to an overestimation of CO_2 adsorption (Figure S53).[42] All these findings demonstrate that by replacing Cu^{2+} with Zn^{2+} centers, we have effectively mitigated the impact of water on the CO_2 sorption capacity of the constructed framework under humid conditions. Interestingly, when the relative CO_2 capacities of the MIP-212s were compared with the benchmark CALF-20 under 20% and 50% RH, a clear difference in humidity tolerance was observed (Supporting Information, Figures S61 and S62). MIP-212(Al/Zn) exhibits a smaller relative loss in CO_2 uptake compared to CALF-20, highlighting its strong tolerance to humidity and its ability to retain a substantial fraction of its dry CO_2 capacity under humid conditions. It should be noted, however, that the CALF-20 values were derived from literature data obtained under slightly different experimental conditions; therefore, this comparison is intended to be indicative of trends rather than a direct quantitative assessment.[46] This shows the ability to rationally tune water affinity and CO_2 capture performance through M^{2+} coordination geometry, without altering the framework topology. While benchmark materials such as CALF-20 hold clear advantages in synthetic maturity and scalability, MIP-212 offers a complementary and transferable design strategy for moisture-tolerant CO_2 capture.

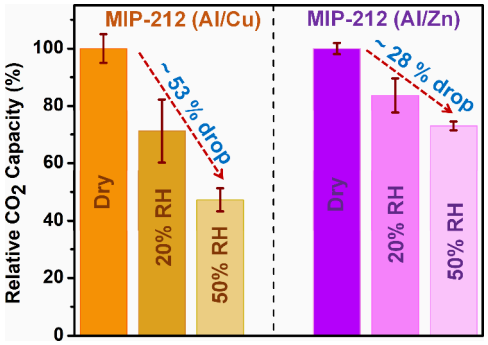

Figure 4. Comparative CO_2 adsorption capacity of MIP-212(Al/Cu) and MIP-212(Al/Zn), under dry and at increasing relative humidity (20% RH and 50% RH) at 1 bar and 303 K.

3. CONCLUSIONS

In the quest for high-performing robust adsorbents for postcombustion CO_2 capture, we designed a novel, robust, bimetallic, heterofunctional (pyrazolate and carboxylate) linker-based MOF, MIP-212(Al/Cu), based on the HSAB principle. MIP-212(Al/Cu) is endowed with infinite Al or Cu based inorganic chains delimiting (i) two types of narrow tunnel-like pores ensuring confinement effect and diffusion of CO_2 molecules while the two different CO_2-philic sites, μ_2–OH groups and Cu open metal sites, offering high CO_2 uptakes and moderate selectivity over nitrogen at 298 K; and (ii) remarkable thermal and water stability. The structure of MIP-212(Al/Cu) before and after activation was successfully determined by *in situ* PXRD methods. Its moderate heat of adsorption (CO_2) value (−36.8 kJ mol^{-1}) as well as its moderate hydrophilic character are both strong assets for future low-energy regeneration processes. Both single-component isotherms and dynamic breakthrough measurements demonstrate that MIP-212(Al/Cu) can act as a high-performer, offering high uptake capacities and desirable selectivity with enhanced stabilities in postcombustion CO_2 capture studies when operated under TSA regeneration conditions, as predicted by the PrISMa platform.

However, its CO_2 sorption capacity decreases under elevated humidity due to the presence of OMS. To mitigate this limitation, we substituted Cu^{2+} with Zn^{2+}, yielding MIP-212(Al/Zn), in which tetrahedral Zn^{2+} coordination eliminates OMS and significantly reduces water interference while retaining μ_2–OH functionality. As a result, MIP-212(Al/Zn) displays superior CO_2 capture performance under 50% RH conditions, confirmed by both single isotherm and breakthrough measurements.

These results establish the MIP-212 platform as a tunable MOF family, where subtle changes in metal composition enable precise control over hydrophilicity and CO_2 sorption properties. Future efforts will focus on either (i) expanding the chemistry of these multifunctional MOFs and (ii) synthesis optimization, scale-up, shaping, and further advanced separation testing under realistic flue-gas conditions, alongside the design of related structures for targeted CO_2 capture and other separation applications.

■ ASSOCIATED CONTENT

Supporting Information

The Supporting Information is available free of charge at https://pubs.acs.org/doi/10.1021/jacs.6c07605.

Details of synthesis protocols of MIP-212(Al/Cu) and MIP-212(Al/Zn); HR-PXRD studies, crystal structure determination and refinement, SEM and EDX results, TGA results, details of activation temperature optimization for both MIP-212(Al/Cu) and MIP-212(Al/Zn) and their characterization analysis (XRD, FTIR, N_2 and CO_2 sorption) results; water stability tests; VT-PXRD

https://doi.org/10.1021/jacs.6c07605
J. Am. Chem. Soc. XXXX, XXX, XXX−XXX

analysis; heat of adsorption and IAST selectivity calculations; comparison of CO_2 sorption capacity of MIP-212 (Al/Cu) with benchmark MOFs for post-combustion CO_2 capture; water sorption analysis; repeatability studies and their characterization analysis results (PXRD and CO_2 sorption); DFT binding energy calculations; FF-GCMC calculations; breakthrough measurements; ssNMR measurements; *in situ* quick X-ray absorption spectroscopy analysis (PDF)

Accession Codes

Deposition Numbers 2545745−2545746 contain the supplementary crystallographic data for this paper. These data can be obtained free of charge via the joint Cambridge Crystallographic Data Centre (CCDC) and Fachinformationszentrum Karlsruhe Access Structures service.

AUTHOR INFORMATION

Corresponding Authors

Georges Mouchaham − *Institut des Matériaux Poreux de Paris, Ecole Normale Supérieure, ESPCI Paris, CNRS, PSL University, Paris 75005, France;* orcid.org/0000-0001-8696-9733; Email: georges.mouchaham@ens.psl.eu

Christian Serre − *Institut des Matériaux Poreux de Paris, Ecole Normale Supérieure, ESPCI Paris, CNRS, PSL University, Paris 75005, France*; Email: christian.serre@ens.psl.eu

Authors

Aysu Yurdusen − *Institut des Matériaux Poreux de Paris, Ecole Normale Supérieure, ESPCI Paris, CNRS, PSL University, Paris 75005, France*

Pratibha Malik − *Institut des Matériaux Poreux de Paris, Ecole Normale Supérieure, ESPCI Paris, CNRS, PSL University, Paris 75005, France*

Asma Mansouri − *Institut des Matériaux Poreux de Paris, Ecole Normale Supérieure, ESPCI Paris, CNRS, PSL University, Paris 75005, France*

Iurii Dovgaliuk − *Institut des Matériaux Poreux de Paris, Ecole Normale Supérieure, ESPCI Paris, CNRS, PSL University, Paris 75005, France;* orcid.org/0000-0003-1997-4748

Matthew Garvin − *The Research Centre for Carbon Solutions (RCCS), School of Engineering and Physical Sciences, Heriot-Watt University, Edinburgh EH14 4AS, U.K.*

Ah-Young Song − *Department of Chemical and Biomolecular Engineering, University of California Berkeley, Berkeley, California 94720, United States; Materials Science Division, Lawrence Berkeley National Laboratory, Berkeley, California 94720, United States*

Alireza Pourghaderi − *Department of Chemical and Biomolecular Engineering, University of California Berkeley, Berkeley, California 94720, United States*

Xin Jin − *Laboratory of Molecular Simulation (LSMO), Institut des Sciences et Ingénierie Chimiques, École Polytechnique Fédérale de Lausanne (EPFL), Sion CH-1951 Valais, Switzerland;* orcid.org/0000-0002-2618-9775

Luke Stuart − *Institut des Matériaux Poreux de Paris, Ecole Normale Supérieure, ESPCI Paris, CNRS, PSL University, Paris 75005, France*

Debanjan Chakraborty − *Institut des Matériaux Poreux de Paris, Ecole Normale Supérieure, ESPCI Paris, CNRS, PSL University, Paris 75005, France*

Shyamapada Nandi − *Institut des Matériaux Poreux de Paris, Ecole Normale Supérieure, ESPCI Paris, CNRS, PSL University, Paris 75005, France*

Lokuge Aravindani Fernando − *The Research Centre for Carbon Solutions (RCCS), School of Engineering and Physical Sciences, Heriot-Watt University, Edinburgh EH14 4AS, U.K.*

Anthony Beauvois − *Synchrotron SOLEIL, Saint-Aubin 91190, France;* orcid.org/0000-0003-0804-8642

Valérie Briois − *Synchrotron SOLEIL, Saint-Aubin 91190, France; UR1-CNRS, Saint Aubin 91190, France*

Jeffrey A. Reimer − *Department of Chemical and Biomolecular Engineering, University of California Berkeley, Berkeley, California 94720, United States; Materials Science Division, Lawrence Berkeley National Laboratory, Berkeley, California 94720, United States*

Susana Garcia − *The Research Centre for Carbon Solutions (RCCS), School of Engineering and Physical Sciences, Heriot-Watt University, Edinburgh EH14 4AS, U.K.;* orcid.org/0000-0002-3713-311X

Berend Smit − *Laboratory of Molecular Simulation (LSMO), Institut des Sciences et Ingénierie Chimiques, École Polytechnique Fédérale de Lausanne (EPFL), Sion CH-1951 Valais, Switzerland;* orcid.org/0000-0003-4653-8562

Complete contact information is available at: https://pubs.acs.org/10.1021/jacs.6c07605

Author Contributions

†A.Y. and P.M. contributed equally.

Notes

The authors declare no competing financial interest.

ACKNOWLEDGMENTS

The authors acknowledge SOLEIL and ESRF synchrotrons for providing beamtime for diffraction and XAS analysis at CRISTAL-SOLEIL (proposal 20200252), ROCK-SOLEIL (proposal 20230561), and BM01-ESRF (SNBL, proposal 20240917) beamlines. The authors are grateful to the staff members of the beamline for their kind assistance. The work at ROCK was supported by a public grant overseen by the French National Research Agency (ANR) as part of the "Investissements d'Avenir" program (Reference: ANR-10-EQPX-45). A.M., G.M., and C.S. acknowledge the Region Ile-de-France in the framework of DIM RESPORE; and A.Y., G.M., and C.S. acknowledge the Agence Nationale de la Recherche under the grant ANR-21-MERA-0006 (MOFAC2-CAP project) for the financial support. P.M., G.M., and C.S. acknowledge funding from the PEPR SPLEEN, CATALPA program, for financial support. We also acknowledge funding from the USorb-DAC Project, supported by a grant from The Grantham Foundation for the Protection of the Environment to RMI's Climate Tech Accelerator programme, Third Derivative. We thank Drs. Hasan Celik, Raynald Giovine, and Pines Magnetic Resonance Center's Core NMR Facility (PMRC Core) for spectroscopic assistance. The instruments used in this work were supported by the PMRC Core. The instrument used in this work is supported by the National Science Foundation under Grant No. 2018784. A.S. gratefully acknowledges support as a Pines Magnetic Resonance Center Postdoctoral Fellow.

https://doi.org/10.1021/jacs.6c07605
J. Am. Chem. Soc. XXXX, XXX, XXX−XXX

■ ABBREVIATIONS

AlF, Al-formate; BET, Brunauer−Emmett−Teller; CALF, Calgary frameworks; CAU, Christian-Albrechts-University; DFT, density functional theory; dobpdc, 4,4′-dioxidobiphenyl-3,3′-dicarboxylate; DMF, *N*,*N*-dimethylformamide; DMSO, dimethyl sulfoxide; DSS, dynamic solvent system; FTIR, Fourier transform infrared; GCMC, grand-canonical Monte Carlo; H2PyC, pyrazole-4-carboxylic acid; HR-PXRD, high-resolution laboratory powder X-ray diffraction; HSAB, hard−soft acids−bases; IAST, ideal adsorbed solution theory; IBU, inorganic building units; IUPAC, International Union of Pure and Applied Chemistry; MIL, Materials of Institute Lavoisier; MIP, Materials from Institute of Porous Materials of Paris; OMS, open metal sites; MOFs, metal−organic frameworks; PyC, pyrazolate-carboxylate; PrISMa, process-informed design of tailor-made sorbent materials; ssNMR, solid-state NMR; TGA, thermal gravimetric analysis; TSA, temperature swing adsorption; TVSA, temperature-vacuum swing adsorption; UFF, universal force field; XAS, X-ray absorption spectroscopy; VT-PXRD, variable-temperature powder X-ray diffraction; SRPXRD, synchrotron powder X-ray diffraction

■ REFERENCES

(1) IEA. *Global Energy and Climate Model*. 2023. https://www.iea.org/reports/global-energy-and-climate-model (accessed 11 June 2024).

(2) IEA. *Carbon Capture, Utilisation and Storage*. https://www.iea.org/energy-system/carbon-capture-utilisation-and-storage#how-does-ccus-work (accessed 11 June 2024).

(3) Choi, S.; Drese, J. H.; Jones, C. W. Adsorbent Materials for Carbon Dioxide Capture from Large Anthropogenic Point Sources. *ChemSusChem* **2009**, *2* (9), 796−854.

(4) Samanta, A.; Zhao, A.; Shimizu, G. K. H.; Sarkar, P.; Gupta, R. Post-Combustion CO2 Capture Using Solid Sorbents: A Review. *Ind. Eng. Chem. Res.* **2012**, *51* (4), 1438−1463. Maurin, G.; Serre, C.; Cooper, A.; Férey, G. The new age of MOFs and of their porous-related solids. *Chem. Soc. Rev.* **2017**, *46* (11), 3104−3107.

(5) Galli, S.; Maspero, A.; Giacobbe, C.; Palmisano, G.; Nardo, L.; Comotti, A.; Bassanetti, I.; Sozzani, P.; Masciocchi, N. When long bis(pyrazolates) meet late transition metals: structure, stability and adsorption of metal−organic frameworks featuring large parallel channels. *Journal of Materials Chemistry A* **2014**, *2* (31), 12208−12221.

(6) Hepburn, C.; Adlen, E.; Beddington, J.; Carter, E. A.; Fuss, S.; Mac Dowell, N.; Minx, J. C.; Smith, P.; Williams, C. K. The technological and economic prospects for CO2 utilization and removal. *Nature* **2019**, *575* (7781), 87−97. Trickett, C. A.; Helal, A.; Al-Maythalony, B. A.; Yamani, Z. H.; Cordova, K. E.; Yaghi, O. M. The chemistry of metal−organic frameworks for CO2 capture, regeneration and conversion. *Nature Reviews Materials* **2017**, *2* (8), 17045. Kim, E. J.; Siegelman, R. L.; Jiang, H. Z. H.; Forse, A. C.; Lee, J.-H.; Martell, J. D.; Milner, P. J.; Falkowski, J. M.; Neaton, J. B.; Reimer, J. A.; et al. Cooperative carbon capture and steam regeneration with tetraamine-appended metal−organic frameworks. *Science* **2020**, *369* (6502), 392−396.

(7) Lin, J.-B.; Nguyen, T. T. T.; Vaidhyanathan, R.; Burner, J.; Taylor, J. M.; Durekova, H.; Akhtar, F.; Mah, R. K.; Ghaffari-Nik, O.; Marx, S.; et al. A scalable metal-organic framework as a durable physisorbent for carbon dioxide capture. *Science* **2021**, *374* (6574), 1464−1469.

(8) Chen, B.; Fan, D.; Pinto, R. V.; Dovgaliuk, I.; Nandi, S.; Chakraborty, D.; García-Moncada, N.; Vimont, A.; McMonagle, C. J.; Bordonhos, M.; et al. A Scalable Robust Microporous Al-MOF for Post-Combustion Carbon Capture. *Advanced Science* **2024**, *11* (21), No. 2401070.

(9) Svante. https://www.svanteinc.com/press-releases/svante-secures-commercial-supply-of-mof-advanced-sorbent-materials-with-basf-for-carbon-capture-market/ (accessed 11 June 2024).

(10) Evans, H. A.; Mullangi, D.; Deng, Z.; Wang, Y.; Peh, S. B.; Wei, F.; Wang, J.; Brown, C. M.; Zhao, D.; Canepa, P.; et al. Aluminum formate, Al(HCOO)3: An earth-abundant, scalable, and highly selective material for CO2 capture. *Science Advances* **2022**, *8* (44), No. eade1473.

(11) Karimi, M.; Siqueira, R. M.; Rodrigues, A. E.; Nouar, F.; Silva, J. A. C.; Serre, C.; Ferreira, A. F. P. Separation of CO2/N2 onto Shaped MOF MIL-160(Al) Using the Pressure Swing Adsorption Process for Post-combustion Application. *Ind. Eng. Chem. Res.* **2024**, *63* (19), 8772−8785.

(12) Henrotin, A.; Heymans, N.; Duprez, M. E.; Mouchaham, G.; Serre, C.; Wong, D.; Robinson, R.; Mulrooney, D.; Casaban, J.; De Weireld, G. Lab-scale pilot for CO2 capture vacuum pressure swing adsorption: MIL-160(Al) vs zeolite 13X. *Carbon Capture Science & Technology* **2024**, *12*, No. 100224.

(13) Nandi, S.; Chakraborty, D.; Daouli, A.; Dovgaliuk, I.; Heymans, N.; Cornu, I.; Florian, P.; De Weireld, G.; Maurin, G.; Nouar, F.et al.Unlocking the scale-up of the benchmark MOFs MIL-53(Al)'s MOFs. *Commun. Mater.***2026**.

(14) Ding, M.; Cai, X.; Jiang, H.-L. Improving MOF stability: approaches and applications. *Chemical Science* **2019**, *10* (44), 10209−10230.

(15) Wang, H.-H.; Jia, L.-N.; Hou, L.; Shi, W.-j.; Zhu, Z.; Wang, Y.-Y. A New Porous MOF with Two Uncommon Metal−Carboxylate−Pyrazolate Clusters and High CO2/N2 Selectivity. *Inorg. Chem.* **2015**, *54* (4), 1841−1846.

(16) Chen, K.-J.; Lin, R.-B.; Liao, P.-Q.; He, C.-T.; Lin, J.-B.; Xue, W.; Zhang, Y.-B.; Zhang, J.-P.; Chen, X.-M. New Zn-Aminotriazolate-Dicarboxylate Frameworks: Synthesis, Structures, and Adsorption Properties. *Cryst. Growth Des.* **2013**, *13* (5), 2118−2123. Mercuri, G.; Moroni, M.; Domasevitch, K. V.; Di Nicola, C.; Campitelli, P.; Pettinari, C.; Giambastiani, G.; Galli, S.; Rossin, A. Carbon Dioxide Capture and Utilization with Isomeric Forms of Bis(amino)-Tagged Zinc Bipyrazolate Metal−Organic Frameworks. *Chem. − Eur. J.* **2021**, *27* (14), 4746−4754.

(17) Zhang, Y.-Z.; He, T.; Kong, X.-J.; Bian, Z.-X.; Wu, X.-Q.; Li, J.-R. Single-Crystal Synthesis and Structures of Highly Stable Ni8-Pyrazolate-Based Metal−Organic Frameworks. *ACS Materials Letters* **2019**, *1* (1), 20−24.

(18) Mosca, N.; Vismara, R.; Fernandes, J. A.; Tuci, G.; Di Nicola, C.; Domasevitch, K. V.; Giacobbe, C.; Giambastiani, G.; Pettinari, C.; Aragones-Anglada, M.; et al. Nitro-Functionalized Bis(pyrazolate) Metal−Organic Frameworks as Carbon Dioxide Capture Materials under Ambient Conditions. *Chem. − Eur. J.* **2018**, *24* (50), 13170−13180.

(19) Chevreau, H.; Permyakova, A.; Nouar, F.; Fabry, P.; Livage, C.; Ragon, F.; Garcia-Marquez, A.; Devic, T.; Steunou, N.; Serre, C.; et al. Synthesis of the biocompatible and highly stable MIL-127(Fe): from large scale synthesis to particle size control. *CrystEngComm* **2016**, *18* (22), 4094−4101.

(20) Kulandaivel, S.; Yang, C.-C.; Yeh, Y.-C.; Lin, C.-H. Defect Induced Structural Transition and Lipase Immobilization in Mesoporous Aluminum Metal-Organic Frameworks. *Chem. − Eur. J.* **2024**, *30* (33), No. e202400603.

(21) Serre, C.; Millange, F.; Thouvenot, C.; Noguès, M.; Marsolier, G.; Louër, D.; Férey, G. Very Large Breathing Effect in the First Nanoporous Chromium(III)-Based Solids: MIL-53 or CrIII(OH)·{O2C−C6H4−CO2}·{HO2C−C6H4−CO2H}x·H2Oy. *J. Am. Chem. Soc.* **2002**, *124* (45), 13519−13526.

(22) Yot, P. G.; Boudene, Z.; Macia, J.; Granier, D.; Vanduyfhuys, L.; Verstraelen, T.; VanSpeybroeck, V.; Devic, T.; Serre, C.; Férey, G.; et al. Metal−organic frameworks as potential shock absorbers: the case of the highly flexible MIL-53(Al). *Chem. Commun.* **2014**, *50* (67), 9462−9464. Mihaylov, M.; Chakarova, K.; Andonova, S.; Drenchev, N.; Ivanova, E.; Sabetghadam, A.; Seoane, B.; Gascon, J.; Kapteijn, F.; Hadjiivanov, K. Adsorption Forms of CO2 on MIL-

https://doi.org/10.1021/jacs.6c07605
J. Am. Chem. Soc. XXXX, XXX, XXX−XXX

53(Al) and NH2-MIL-53(Al) As Revealed by FTIR Spectroscopy. *J. Phys. Chem. C* **2016**, *120* (41), 23584−23595. Stavitski, E.; Pidko, E. A.; Couck, S.; Remy, T.; Hensen, E. J. M.; Weckhuysen, B. M.; Denayer, J.; Gascon, J.; Kapteijn, F. Complexity behind CO2 Capture on NH2-MIL-53(Al). *Langmuir* **2011**, *27* (7), 3970−3976.

(23) Cadiau, A.; Lee, J. S.; DamascenoBorges, D.; Fabry, P.; Devic, T.; Wharmby, M. T.; Martineau, C.; Foucher, D.; Taulelle, F.; Jun, C.-H.; et al. Design of Hydrophilic Metal Organic Framework Water Adsorbents for Heat Reallocation. *Adv. Mater.* **2015**, *27* (32), 4775−4780. Sánchez-Serratos, M.; Bayliss, P. A.; Peralta, R. A.; González-Zamora, E.; Lima, E.; Ibarra, I. A. CO2 capture in the presence of water vapour in MIL-53(Al). *New J. Chem.* **2016**, *40* (1), 68−72.

(24) Ramsahye, N. A.; Maurin, G.; Bourrelly, S.; Llewellyn, P.; Loiseau, T.; Ferey, G. Charge distribution in metal organic framework materials: transferability to a preliminary molecular simulation study of the CO2 adsorption in the MIL-53 (Al) system. *Phys. Chem. Chem. Phys.* **2007**, *9* (9), 1059−1063.

(25) Reinsch, H.; Waitschat, S.; Stock, N. Mixed-linker MOFs with CAU-10 structure: synthesis and gas sorption characteristics. *Dalton Transactions* **2013**, *42* (14), 4840−4847.

(26) Zhang, J.-P.; Zhang, Y.-B.; Lin, J.-B.; Chen, X.-M. Metal Azolate Frameworks: From Crystal Engineering to Functional Materials. *Chem. Rev.* **2012**, *112* (2), 1001−1033. Wang, K.; Lv, X.-L.; Feng, D.; Li, J.; Chen, S.; Sun, J.; Song, L.; Xie, Y.; Li, J.-R.; Zhou, H.-C. Pyrazolate-Based Porphyrinic Metal−Organic Framework with Extraordinary Base-Resistance. *J. Am. Chem. Soc.* **2016**, *138* (3), 914−919. Colombo, V.; Galli, S.; Choi, H. J.; Han, G. D.; Maspero, A.; Palmisano, G.; Masciocchi, N.; Long, J. R. High thermal and chemical stability in pyrazolate-bridged metal−organic frameworks with exposed metal sites. *Chemical Science* **2011**, *2* (7), 1311−1319.

(27) Heering, C.; Boldog, I.; Vasylyeva, V.; Sanchiz, J.; Janiak, C. Bifunctional pyrazolate−carboxylate ligands for isoreticular cobalt and zinc MOF-5 analogs with magnetic analysis of the {Co4(μ4-O)} node. *CrystEngComm* **2013**, *15* (45), 9757−9768. Bian, Z.-X.; Zhang, Y.-Z.; Tian, D.; Zhang, X.; Xie, L.-H.; Zhao, M.; Xie, Y.; Li, J.-R. Co7-Cluster-Based Metal−Organic Frameworks with Mixed Carboxylate and Pyrazolate Ligands: Construction and CO2 Adsorption and Fixation. *Cryst. Growth Des.* **2020**, *20* (12), 7972−7978. Zheng, Q.; Yang, F.; Deng, M.; Ling, Y.; Liu, X.; Chen, Z.; Wang, Y.; Weng, L.; Zhou, Y. A Porous Metal−Organic Framework Constructed from Carboxylate−Pyrazolate Shared Heptanuclear Zinc Clusters: Synthesis, Gas Adsorption, and Guest-Dependent Luminescent Properties. *Inorg. Chem.* **2013**, *52* (18), 10368−10374.

(28) Si, G.; Kong, X.; He, T.; Wu, W.; Xie, L.; Li, J. A stable Co(II)-based metal-organic framework with dual-functional pyrazolate-carboxylate ligand: Construction and CO2 selective adsorption and fixation. *Chin. Chem. Lett.* **2021**, *32* (2), 918−922. Menzel, S.; Höfert, S.-P.; Öztürk, S.; Schmitz, A.; Janiak, C. A mixed-valence copper(I/II) coordination polymer directed with a bifunctional soft-hard pyrazolate−carboxylate ligand. *Zeitschrift für anorganische und allgemeine Chemie* **2021**, *647* (8), 803−808. Lancheros, A.; Goswami, S.; Mian, M. R.; Zhang, X.; Zarate, X.; Schott, E.; Farha, O. K.; Hupp, J. T. Modulation of CO2 adsorption in novel pillar-layered MOFs based on carboxylate−pyrazole flexible linker. *Dalton Transactions* **2021**, *50* (8), 2880−2890.

(29) Zhou, L.; Brântuas, P.; Henrique, A.; Reinsch, H.; Wahiduzzaman, M.; Grenèche, J.-M.; Rodrigues, A. E.; Silva, J. A. C.; Maurin, G.; Serre, C. A Microporous Multi-Cage Metal−Organic Framework for an Effective One-Step Separation of Branched Alkanes Feeds. *Angew. Chem., Int. Ed.* **2024**, *63* (15), No. e202320008.

(30) Yu, J.; Xie, L.-H.; Li, J.-R.; Ma, Y.; Seminario, J. M.; Balbuena, P. B. CO2 capture and separations using MOFs: computational and experimental studies. *Chem. Rev.* **2017**, *117* (14), 9674−9754.

(31) Charalambous, C.; Moubarak, E.; Schilling, J.; Sanchez Fernandez, E.; Wang, J.-Y.; Herraiz, L.; McIlwaine, F.; Peh, S. B.; Garvin, M.; Jablonka, K. M.; et al. A holistic platform for accelerating sorbent-based carbon capture. *Nature* **2024**, *632* (8023), 89−94.

(32) Alezi, D.; Oppenheim, J. J.; Sarver, P. J.; Iliescu, A.; Dinakar, B.; Dincă, M. Tunable Low−Relative Humidity and High−Capacity Water Adsorption in a Bibenzotriazole Metal−Organic Framework. *J. Am. Chem. Soc.* **2023**, *145* (46), 25233−25241.

(33) Xu, G.; Peng, Y.; Hu, Z.; Yuan, D.; Donnadieu, B.; Zhao, D.; Cheng, H. A 2D metal−organic framework composed of a bi-functional ligand with ultra-micropores for post-combustion CO2 capture. *RSC Adv.* **2015**, *5* (59), 47384−47389.

(34) Dong, K.; Zhai, Z.; Guo, A. Effects of pore parameters and functional groups in coal on CO2/CH4 adsorption. *ACS omega* **2021**, *6* (48), 32395−32407. Su, S.; Zhang, Y.; Zhu, M.; Song, X.; Wang, S.; Zhao, S.; Song, S.; Yang, X.; Zhang, H. An active-site-accessible porous metal−organic framework composed of triangular building units: preparation, catalytic activity and magnetic property. *Chem. Commun.* **2012**, *48* (90), 11118−11120.

(35) Grzywa, M.; Denysenko, D.; Schaller, A.; Kalytta-Mewes, A.; Volkmer, D. Flexible chiral pyrazolate-based metal−organic framework containing saddle-type Cu I 4 (pyrazolate) 4 units. *CrystEngComm* **2016**, *18* (40), 7883−7893.

(36) Cingolani, A.; Galli, S.; Masciocchi, N.; Pandolfo, L.; Pettinari, C.; Sironi, A. Sorption− desorption behavior of bispyrazolato−copper (II) 1D coordination polymers. *J. Am. Chem. Soc.* **2005**, *127* (17), 6144−6145.

(37) Liu, Q.; Song, Y.; Ma, Y.; Zhou, Y.; Cong, H.; Wang, C.; Wu, J.; Hu, G.; O'Keeffe, M.; Deng, H. Mesoporous cages in chemically robust MOFs created by a large number of vertices with reduced connectivity. *J. Am. Chem. Soc.* **2019**, *141* (1), 488−496.

(38) Loiseau, T.; Serre, C.; Huguenard, C.; Fink, G.; Taulelle, F.; Henry, M.; Bataille, T.; Férey, G. A Rationale for the Large Breathing of the Porous Aluminum Terephthalate (MIL-53) Upon Hydration. *Chem. − Eur. J.* **2004**, *10* (6), 1373−1382.

(39) Jia, Y.-Y.; Liu, X.-T.; Feng, R.; Zhang, S.-Y.; Zhang, P.; He, Y.-B.; Zhang, Y.-H.; Bu, X.-H. Improving the Stability and Gas Adsorption Performance of Acylamide Group Functionalized Zinc Metal−Organic Frameworks through Coordination Group Optimization. *Cryst. Growth Des.* **2017**, *17* (5), 2584−2588. Zhang, Y.-Z.; He, T.; Lv, X.-L.; Wang, B.; Xie, L.-H.; Liu, X.-M.; Li, J.-R. Nanocage containing metal-organic framework constructed from a newly designed low symmetry tetra-pyrazole ligand. *J. Coord. Chem.* **2016**, *69* (21), 3242−3249. Campitelli, P.; Tombesi, A.; DiNicola, C.; Pettinari, C.; Mauri, A.; Galli, S.; Yan, T.; Liu, D.; Duan, J. D.; Goswami, S.; et al. CO2 Capture and Conversion to C1 Chemicals with Mixed-Metal Copper/Nickel Bis(amino)bipyrazolate Metal−Organic Frameworks. *ACS Appl. Energy Mater.* **2023**, *6* (18), 9231−9242. Vismara, R.; Tuci, G.; Tombesi, A.; Domasevitch, K. V.; DiNicola, C.; Giambastiani, G.; Chierotti, M. R.; Bordignon, S.; Gobetto, R.; Pettinari, C.; et al. Tuning Carbon Dioxide Adsorption Affinity of Zinc(II) MOFs by Mixing Bis(pyrazolate) Ligands with N-Containing Tags. *ACS Appl. Mater. Interfaces* **2019**, *11* (30), 26956−26969.

(40) Biswas, S.; Ahnfeldt, T.; Stock, N. New Functionalized Flexible Al-MIL-53-X (X = -Cl, -Br, -CH3, -NO2, -(OH)2) Solids: Syntheses, Characterization, Sorption, and Breathing Behavior. *Inorg. Chem.* **2011**, *50* (19), 9518−9526.

(41) Yazaydın, A. Ö.; Benin, A. I.; Faheem, S. A.; Jakubczak, P.; Low, J. J.; Willis, R. R.; Snurr, R. Q. Enhanced CO2 Adsorption in Metal-Organic Frameworks via Occupation of Open-Metal Sites by Coordinated Water Molecules. *Chem. Mater.* **2009**, *21* (8), 1425−1430. Soubeyrand-Lenoir, E.; Vagner, C.; Yoon, J. W.; Bazin, P.; Ragon, F.; Hwang, Y. K.; Serre, C.; Chang, J.-S.; Llewellyn, P. L. How Water Fosters a Remarkable 5-Fold Increase in Low-Pressure CO2 Uptake within Mesoporous MIL-100(Fe). *J. Am. Chem. Soc.* **2012**, *134* (24), 10174−10181.

(42) Li, Y.; Jin, X.; Moubarak, E.; Smit, B. A Refined Set of Universal Force Field Parameters for Some Metal Nodes in Metal−Organic Frameworks. *J. Chem. Theory Comput.* **2024**, *20* (23), 10540−10552.

(43) Feng, C.; Zhao, H.; Li, Z.-Q. Highly efficient electrochemiluminescence on microporous MOFs containing zinc secondary building units with a pcu net. *J. Solid State Chem.* **2018**, *258*, 841−844.

https://doi.org/10.1021/jacs.6c07605
J. Am. Chem. Soc. XXXX, XXX, XXX−XXX

(44) Canivet, J.; Bonnefoy, J.; Daniel, C.; Legrand, A.; Coasne, B.; Farrusseng, D. Structure−property relationships of water adsorption in metal−organic frameworks. *New J. Chem.* **2014**, *38* (7), 3102−3111. Canivet, J.; Fateeva, A.; Guo, Y.; Coasne, B.; Farrusseng, D. Water adsorption in MOFs: fundamentals and applications. *Chem. Soc. Rev.* **2014**, *43* (16), 5594−5617.

(45) Massiot, D.; Fayon, F.; Capron, M.; King, I.; Le Calvé, S.; Alonso, B.; Durand, J.-O.; Bujoli, B.; Gan, Z.; Hoatson, G. Modelling one- and two-dimensional solid-state NMR spectra. *Magn. Reson. Chem.* **2002**, *40* (1), 70−76.

(46) Constant, N.; Liske, G.; Ravuru, S. S.; Puliyanda, A.; Pugnet, V.; Orsikowsky Sanchez, A.; Chavan, S. R.; Llewellyn, P.; Sawada, J. A.; Rajendran, A. Binary CO2/H2O Adsorption on CO2 Capture Metal−Organic Frameworks CALF-20, Al-Fumarate and CAU-10-H Using Microscale Dynamic Column Breakthrough. *Ind. Eng. Chem. Res.* **2025**, *64* (3), 1712−1729.

https://doi.org/10.1021/jacs.6c07605
J. Am. Chem. Soc. XXXX, XXX, XXX−XXX